Clay Minerals, (2011) **46**, 47–58

Influence of hydrocarbon contamination on clay soil microstructure

D. IZDEBSKA-MUCHA[1], J. TRZCIŃSK[1], M. S. ŻBIK[2] AND R. L. FROST[2,*]

[1] *Institute of Hydrogeology and Engineering Geology, Faculty of Geology, University of Warsaw, Żwirki i Wigury 93, Warsaw, 02-089, Poland, and* [2] *Chemistry Discipline, Faculty of Science and Technology, Queensland University of Technology, 2 George Street, GPO Box 2434, Brisbane, Queensland 4001, Australia*

(*Received 25 February 2010; revised 16 August 2010; Editor: Balwant Singh*)

ABSTRACT: Microstructural (fabric, forces and composition) changes due to hydrocarbon contamination in a clayey soil (glacial till) were studied using scanning electron microscopy (micro-fabric analysis), atomic force microscopy (force measurement) and a sedimentation bench test (particle size measurements). Non-polluted and polluted glacial till from NE Poland (in the area of a fuel terminal) were used for the study. Electrostatic repulsive forces in the polluted samples were much lower than in non-polluted samples. In comparison with non-polluted samples, the polluted samples exhibited lower electric charge, attractive forces on approach and strong adhesion on withdrawal. The results of the sedimentation tests indicate that clay particles form larger aggregates and settle out of the suspension rapidly in diesel oil. In non-polluted soil, the fabric is strongly aggregated – dense packing, dominating face-to-face and edge-to-edge types of contacts, clay film tightly adhering to the surface of larger grains and interparticle pores are more common. In polluted soil the clay matrix is less aggregated – loose packing, dominating edge-to-face types of contacts and inter-micro-aggregate pores are more frequent. Substantial differences were observed in the morphometric and geometrical parameters of the pore space. The polluted soil micro-fabric proved to be more isotropic and less oriented than in non-polluted soil. The polluted soil, in which electrostatic forces were suppressed by hydrocarbon interaction, displays more open porosity and larger voids than non-polluted soil, which is characterized by the occurrence of strong electrostatic interaction between the clay particles.

KEYWORDS: clay soil, fabric, interparticle forces, petroleum pollution, particle size.

Petroleum and its products constitute one of the most prevalent sources of environmental pollution. Such materials are released in accidental spills during transportation both on land and sea from tankers and pipelines, for instance at sites where the oil is extracted and as leakages from underground storage tanks and distribution facilities. Petroleum-derived contaminants also collect in wastewater from urban and industrial areas. In some cases oil spills might be caused deliberately during war conflicts. The majority of petroleum pollution arises from non-point sources such as small, usually unreported, spills and leakages, often of unknown localization (Riser-Roberts, 1998; Surygała & Śliwka, 1999; www.pollutionissues.com/Na-Ph/Petroleum.html). Small amounts of the pollutant are regularly released, which over a long period of time add up to a large-scale contamination of the subsurface soil and ground water. Based on the grain-size distribution, the most sensitive environments to the contamination are clay soils. For clay particles the sensitivity index is 0.6–0.9 (Fang, 1997).

* E-mail: r.frost@qut.edu.au
DOI: 10.1180/claymin.2011.046.1.47

Contamination of a soil by petroleum substances, characterized by physicochemical properties different from water, was found to have a deteriorating effect on its physical, mechanical and filtration parameters (Bowders & Daniel, 1987; Fernandez & Quigley, 1988; Uppot & Stephenson, 1989; Izdebska-Mucha, 2005; Korzeniowska-Rejmer & Izdebska-Mucha, 2006; Khamehchiyan *et al*., 2007; Singh *et al*., 2009).

The engineering properties of clay soils are strongly dependent on soil microstructure. The term 'microstructure' is frequently used in many fields of material sciences as well as in soil engineering. Microstructure is defined in this context as soil fabric and composition, and interparticle forces between structural elements. This concept was described for example by Mitchell (1976) and Gillott (1987).

The term 'fabric' refers to the arrangement of particles, particle groups (microaggregates and aggregates) and pore space in soils. The composition of soils comprises: type of minerals and their amount; type of adsorbed cations; pore water composition; and shapes and size distribution of particles. Primary microstructures form on deposition (sedimentation processes) and change to secondary microstructures as a result of many factors in the geological history of soils.

Results reported on the fabric of contaminated soils are limited to qualitative descriptions of samples obtained after filtration tests or suspension studies (e.g. Fernandez & Quigley, 1985; Berger *et al*., 2002; Kaya & Fang, 2005). Kaya & Fang (2000, 2005) investigated physicochemical properties and interparticle force systems of clays with different organic pore fluids. They concluded analytically that both repulsive and attractive forces decreased as the dielectric constant of the pore fluid decreased; however, no experimental confirmation was published on the contaminated soil environment and the present work contributes to closing this knowledge gap.

This study contributes to understanding the mechanisms causing changes in soil microstructure after pollution by petroleum substances. The quantitative characteristics of pore space parameters along with a qualitative description were determined using STIMAN, the special software for the micrograph analysis. The STIMAN image analyser (Sergeyev *et al*., 1983; Sokolov *et al*., 2002) has a unique feature which allows a study of polydispersed samples. It processes and interprets a series of SEM images at different magnifications, which covers the entire range of particle and aggregate sizes under investigation.

The interparticle forces were directly measured on clay particles separated from natural clean and contaminated clay soil.

MATERIALS AND METHODS

Clay soil

The natural clayey soil used for this study was a glacial till from NE Poland. The soil samples were collected from the area of a fuel terminal where an accidental spillage of diesel oil occurred from underground fuel tanks. In the area where downflow and stagnation of diesel oil took place, petroleum-derived substances migrated upwards in the soil causing pollution up to the groundwater level. The hydrocarbon content at a depth of 2 m was 5395 [mg kg^{-1} dry weight] which was the sum of shorter chain C_6–C_{12} (1457 mg kg^{-1} dry weight) and longer chain > C_{12} (3938 mg kg^{-1} dry weight) hydrocarbons.

Soil samples were taken from two pits located respectively in polluted and unaffected areas. The distance between the pits was of about 50 m and the samples were collected ten months after the pollution incident. The soil samples have been named: NP – unpolluted soil and P – polluted soil. The grain-size distribution of the studied soil was: sand 54%, silt 25% and clay 21%, which gave this soil sample the classification as: sandy clay with silt (BS, 1990), CL (ASTM, 2006). The plastic limit was 15%, the liquid limit 30%, the specific density 2.69 g cm^{-3} (obtained using a gas pycnometry method), the specific surface area 24 m^2 g^{-1} and the cation exchange capacity (CEC) 3.09 meq/100g (obtained using the methylene blue adsorption method).

Force measurements

The force measurements, as described earlier (Ducker *et al*., 1991) were conducted using atomic force microscopy (AFM) with a Nanoscope III atomic force microscope, Digital Instruments, Santa Barbara. A force mode with scan head E rate between 0.3 and 3 μm s^{-1} was applied. The measurements were made on 200 μm long, wide V-shaped Si_3N_4 colloidal probe cantilevers.

The spring constant of the cantilever was 0.12 N m^{-1}. The force resolution of the AFM is

about 1−0.1 nN with the separation distance resolution of ~0.01 nm. The clay-coated flat substrate surface was displaced in a controlled manner towards and away from the clay-topped probe in aqueous solutions. The interacting forces between the probe and the flat surface were obtained from the deflection of the cantilever. The deflection of the cantilever *vs*. the displacement of the flat surface was converted into surface force *vs.* separation by assuming that the zero point of separation was defined as the compliance region where the probe and the flat surface are in contact and the zero force is determined at large surface separations. The force measurements were carried out at a scan rate of 1 Hz over a scanning distance from 200 to 500 nm and were carried out in demineralized water purified by a Milli-Q filtration system and in 0.01 and 0.1 M KCl solutions. Salts used in this work were analytical grade. For force measurements, the dry samples were re-dispersed in water using an ultrasonic bath. The dispersion of the clay samples was prepared from 0.2 wt.% of the dry mass of the size fraction below 1 μm as recommended in previous work (Żbik & Frost, 2010). A micro-drop of suspension was placed on the probe and a few drops on the substrate (silicon wafer) to produce the clay-topped surface, followed by drying in a laminar flow cabinet at room temperature overnight. Both surfaces were heated at a temperature of 80ºC to stick the clay flakes firmly onto the sphere and substrate surfaces.

AFM investigation on the oriented clay layers on top of the silicon wafer was chosen because it is very hard to locate the individual clay platelets and to position the colloidal probe directly over the clay platelets. In part this is due to the small difference in refractive index between different clay crystals and water, leading to a small optical contrast and visibility of the platelet under water; in part this is due to the mechanical arrangement of the AFM.

The thickness of the clay film was not measured but the force measured was between the spherical probe and the clay sample colloidal film deposited on the silicon wafer. Force F (normalized by the spherical probe's radius of curvature R) is plotted on a logarithmic scale against the minimum distance D from the sphere's surface to the flat plate. This is the standard way of plotting surface force measurements, since the quantity F/R should be independent of the sphere's radius and, consequently, data from different experiments can be compared.

A Panalytical X'Pert PRO X-ray diffraction (XRD) unit was used with Cu-$K\alpha$ radiation at 40 kV and 40 mA. The sample was scanned for 12 min over the 2θ interval 3−35º using a post-diffraction monochromator and a multi-wire detector. The XRD diffraction patterns of the NP clay colloidal sample (not shown in this contribution) confirm a mixture of illite, kaolinite and smectite with a trace amount of quartz.

Sedimentation test

The soils for the sedimentation test were prepared using a modified method given by Moavenian & Yasrobi (2008). Fine particles passing a 63 μm sieve were separated from the NP soil by wet sieving. The material was air-dried and powdered. Two samples of 15 g each were placed in 250 ml beakers, covered with 125 ml of deionized water and diesel oil respectively, and left for 24 h. After soaking, the samples were dispersed with a magnetic stirrer for 20 min (speed range 200 rpm), transferred into glass sedimentation cylinders and made up to 1000 ml with deionized water and diesel oil respectively. Hydrometer measurements of soil−water and soil−diesel oil suspensions were then carried out according to the BS (1990) and ASTM (1990) procedures.

Analysis of fabric

Microscope studies were carried out using a high-resolution scanning electron microscope (SEM), JEOL model JSM 6380 LA. From untreated samples of NP and P till, ~1 cm^3 cubes were cut and dried using a low-temperature freeze-drying method (Tovey & Wong, 1973; Smart & Tovey, 1982). The qualitative description of fabrics was based on the images magnified from $100\times$ to $6500\times$. The same images were analysed quantitatively using an image analyser and the structural image analysis (STIMAN) software package. The morphometric and geometrical parameters were calculated according to the methods given by Sergeyev *et al*. (1983), Sokolov *et al*. (2002) and Trzciński (2004). The main type of microstructure, the character of contacts between structural elements and the pore space classification were named following the convention suggested by Sergeyev *et al*. (1978, 1980) and Grabowska-Olszewska *et al*. (1984), supplemented by Trzciński (2008).

RESULTS AND DISCUSSION

Sedimentation test

The results of the sedimentation test are presented in Fig. 1. The soil particles in the diesel oil suspension settled out much faster than in water. When preparing the suspensions in the sedimentation cylinders it was macroscopically observed that in diesel oil the soil particles were coarser than in water, even though initially sampled from the same soil material. The test lasted six days and the suspensions presented different sedimentation patterns. During all the experiment, the water suspension stayed dense and non-transparent, while in diesel oil the sedimentation began more rapidly and the suspension became relatively clear after a few hours. At the end of the test, 100% of soil particles settled out of diesel oil, while in water the sedimentation figure was 75%. These findings are in agreement with an earlier study by Moavenian & Yasrobi (2008), who showed that the percentage sedimentation of a clay decreased in organic liquids of low dielectric constant.

Diesel oil is a fluid of low dielectric constant ($\varepsilon \sim 2$). As shown in earlier papers (Kaya & Fang, 2000, 2005), and directly measured in the AFM experiment presented here, organic liquids of a lower dielectric constant than water significantly alter the surface properties of the clay particles. The results of the sedimentation test indicate that diesel oil pollution in clays which contain soil will alter their aggregation, pore space and microstructure.

Characteristics of the micro-fabric

The qualitative description. Preliminary characterization of the NP and P soil micro-fabric was carried out by Izdebska-Mucha & Trzciński (2008). Taking into account the relative packing of structural elements, the NP soil is characterized, in general, by a comparatively medium packed matrix microstructure (Trzciński, 2008) as illustrated in Fig. 2 (A1, B1 and C1). A clayey matrix (thin arrow in Fig. 2, A1) surrounds individual sandy and silty grains (bold lower arrow in Fig. 2, A1). The clayey matrix is aggregated and is composed of microaggregates (surrounded by a dashed line in Fig. 2, B1) which, together with grains, form clayey-silty and clayey-sandy aggregates. The grain surface is covered with a clay film (thin upper arrow in Fig. 2, C1). The contacts between the microaggregates are of three types; face-to-face FF (bold lower arrow in Fig. 2, C1), edge-to-face EF (bold upper arrow in Fig. 2, C1) or edge-to-edge EE (thin lower arrow in Fig. 2, C1). The orientation of the structural elements is noticeable (Fig. 2, A1, and Fig. 3, A). The pore space is composed mainly of intermicroaggregate pores (bold arrows in Fig. 2, B1), interparticle pores (thin right arrow in Fig. 2, C1) and subordinate inter-aggregate pores (bold upper arrows in Fig. 2, A1).

Significant micro-fabric differences have been noted between P and NP soils, the comparison of their features being given in Fig. 2 (A2, B2 and C2). The clayey matrix is relatively strongly aggregated with clay particles forming aggregates; microaggregates are densely packed in the NP soil – compare Fig. 2 (B1 and 2B2). Between microaggregates, predominant contacts are of the FF and EF type and the clayey film adheres tightly to the surface of sandy and silty grains. In comparison with the NP soil, the clayey matrix is less aggregated and structural elements are more loosely packed in the P soil (Fig. 2, B2).

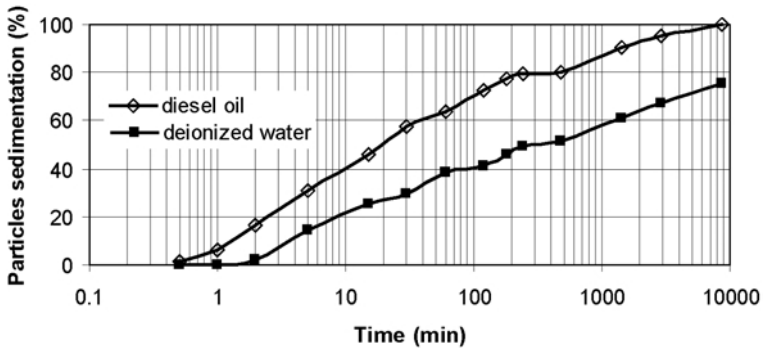

FIG. 1. Sedimentation pattern for the soil in deionized water and diesel oil.

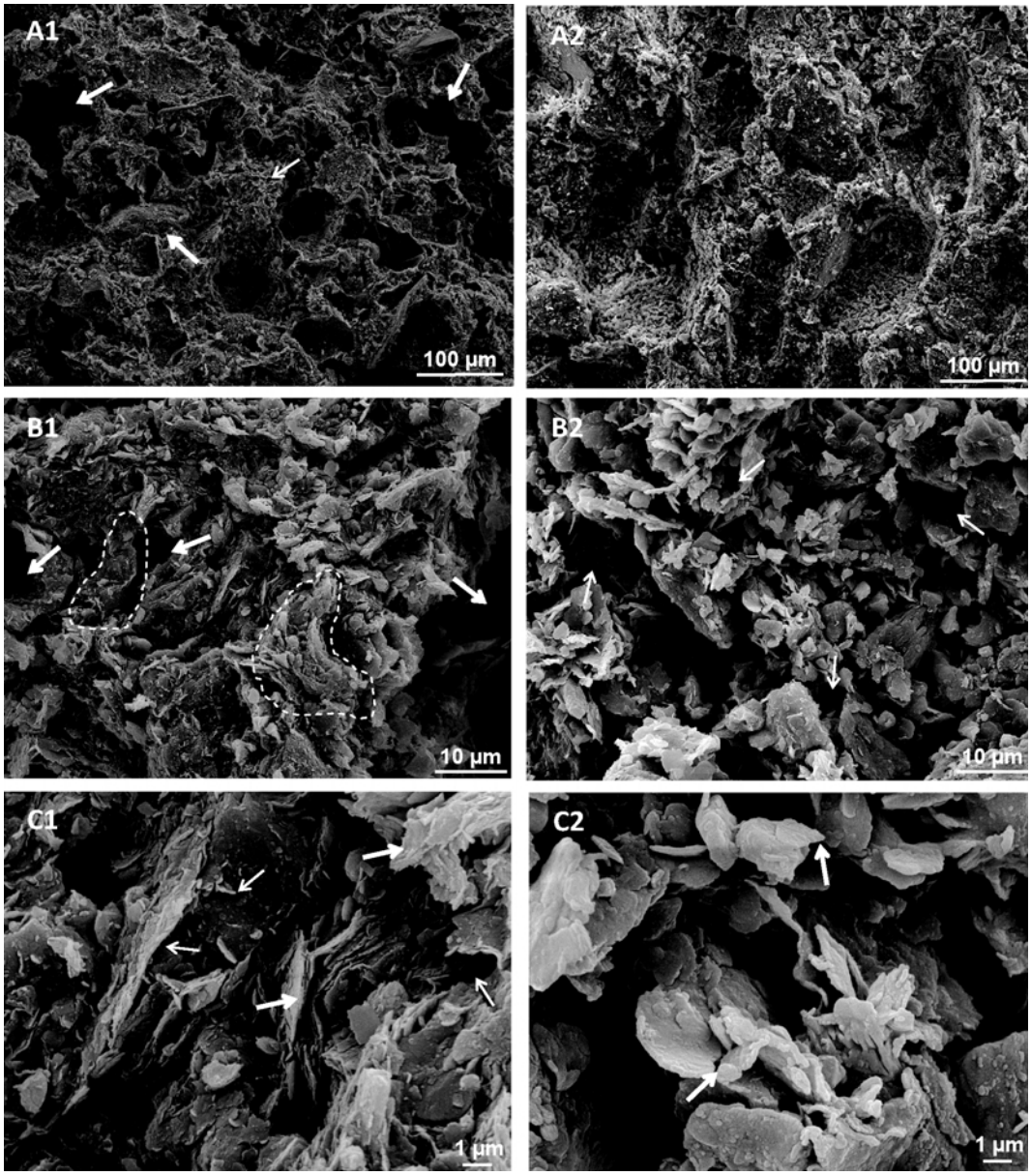

FIG. 2. Fabric changes in NP (unpolluted, SEM micrographs A1, B1, C1) and P (polluted, SEM micrographs A2, B2, C2) clay soil. Magnification: A, 200 ×; B, 1600 ×; C, 6500 ×.

Predominant contacts between clayey microaggregates are of the EF type (bold arrows in Fig. 2, C2). Interparticle pores are more common in the NP soil while, for P soil, intermicroaggregate pores are more frequent (thin arrows in Fig. 2, B2). The surface of the NP sample is smoother than the rough surface of the P sample (compare Fig. 2, A1 and A2).

The quantitative image analysis. The results of pore space characteristic of NP and P soils are presented in Table 1 and Fig. 3. Substantial differences have been observed in the morphometric

TABLE 1. Quantitative pore space parameters of NP (unpolluted clay soil) and P (clay soil polluted by diesel oil).

	Unpolluted clay soil NP[1]				Polluted clay soil P[2]			
	Min.	Max.	Average value	Standard deviation	Min.	Max.	Average value	Standard deviation
Porosity n (%)	19.2	30.8	24.9	4.64	21.5	26.8	24.4	2.12
Number of pores $N \times 10^3$	178	1,503	730	456	265	752	420	195
Total pore area $S_t \times 10^3$ (μm^2)	446	2,866	2,102	882	1,979	2,530	2,276	210
Maximum pore area S_{max} (μm^2)	9,356	130,565	92,301	48,697	43,782	375,622	140,862	135,013
Average pore area S_{av} (μm^2)	1.91	4.65	3.15	0.96	3.36	8.99	6.09	2.04
Total pore perimeter $P_t \times 10^3$ (μm)	1,105	7,932	4,027	2,298	2,240	4,267	2,689	884
Maximum pore perimeter P_{max} (μm)	2,320	15,131	9,900	4,554	8,089	27,827	15,032	7,920
Minimum pore perimeter P_{min} (μm)	1.23	1.41	1.37	0.08	1.32	1.58	1.41	0.12
Average pore perimeter P_{av} (μm)	5.28	6.53	5.73	0.53	5.68	8.52	6.74	1.28
Maximum pore diameter D_{max} (μm)	109	408	326	118	236	692	392	179
Average pore diameter D_{av} (μm)	0.70	0.92	0.80	0.08	0.8	1.13	0.93	0.15
Micropores $0.1<\varnothing<10$ μm (%)	24.6	46.9	31.6	9.2	17.3	30.8	21.4	5.5
Mesopores $10<\varnothing<1000$ μm (%)	53.1	75.4	68.5	9.2	69.2	82.7	78.6	5.5
Average form index K_{fav} (−)[3]	0.34	0.429	0.398	0.032	0.399	0.458	0.421	0.028
Isometric pores a/b<1.5 (%)	10.8	13.2	12.2	1.0	9.5	17.4	12.4	3.1
Anisometric pores 1.5<a/b<10 (%)	84.8	88.3	85.9	1.3	80.8	88.9	86.4	3.2
Fissure-like pores a/b>10 (%)	0.6	3.0	2.0	1.0	0.2	2.7	1.3	1.0

[1] Number of tests 6
[2] Number of tests 5
[3] Fissure-like pores: $0<K_f<0.15$; anisometric pores: $0.15<K_f<0.65$; isometric pores: $0.65<K_f<1$
$\varnothing$ The equivalent diameter of pore
a/b The ratio between the two most different dimensions of pore

(area, perimeter, diameter) and geometrical (shape, anisotropy, degree of orientation) parameters between the NP and P soils. The porosity value remains unchanged, but the minimum value is greater for the P soil. The number of pores is smaller in P and the maximum value is much greater in the NP soil.

An analysis of morphometric parameters has provided the following information. There is no significant change in the total pore area of the P soil, whereas the maximum and average pore area parameters clearly shift towards the greater values. The total pore perimeter is smaller but the maximum, minimum and average values of this parameter are greater for the P soil. Elevated maximum and average pore diameter parameters have been found for the P soil. The distribution of pore sizes has changed substantially. The number of micropores has decreased while mesopores proved more abundant in the P soil.

In addition, geometrical parameters have also changed. The average form index value increased in till P. Observations of the pore shape revealed a smaller number of fissure pores with an increased number of anisometric and isometric pores. The anisotropy index value decreased markedly for the P soil (Fig. 3).

A noticeable drop in pore numbers in the P soil coupled with a much lower maximum value of this parameter and no changes in the porosity suggests significant qualitative and quantitative changes in the pore space of the polluted soil. These changes have been confirmed by the distribution of morphometric parameters. The number of micropores decreased with the growth of the number of mesopores in the P soil. The redistribution of pore space in favour of larger pores resulted in an increase in the maximum and average pore area, maximum, minimum and average pore perimeter, maximum and average pore diameter and in a considerable drop in the total pore perimeter value in the P soil.

Changes in shape and orientation of the pores are reflected in the geometrical parameter values. The increase of the form index in the P soil results from an increase in the number of pores of more isometric shape, which is confirmed by a decrease in the number of fissure pores and more abundant isometric and anisometric pores. The change of void shape into a more isometric form is responsible for a significant drop in the anisotropy index in the P soil. Due to the subsequent reorientation of particles and micro-aggregates, the contaminated soil becomes more isotropic.

Force measurements

The results of the test force measurements were obtained using a bare spherical silica glass probe against the mica surface in water and 0.01 M and 0.1 M KCl solutions. As a result of these measurements, a rough comparison can be drawn over what thickness of the double layer can be detected as a repulsive electrostatic force in solutions of certain ionic strength. Test results were plotted in diagrams shown in Fig. 4.

In the force–separation curves (Fig. 4), a long-range repulsion has been recorded whose range decreases as the salt concentration increases. This is the signature of double-layer repulsion. Its presence indicates that the clay/water interface must be negatively charged.

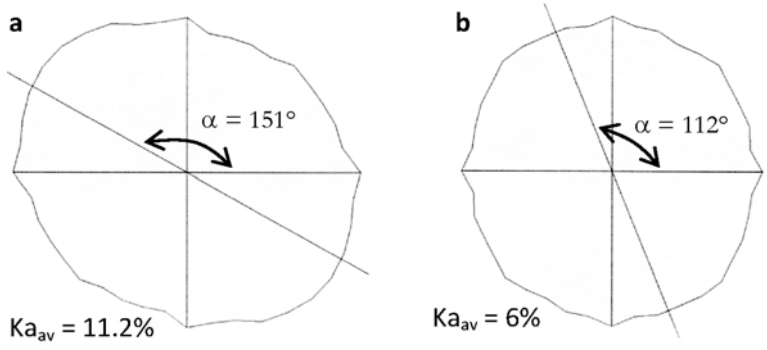

FIG. 3. Examples of orientation diagrams and average values of anisotropy coefficient (Ka_{av}) for NP soil (a) and P soil (b); α, angle of structural elements orientation.

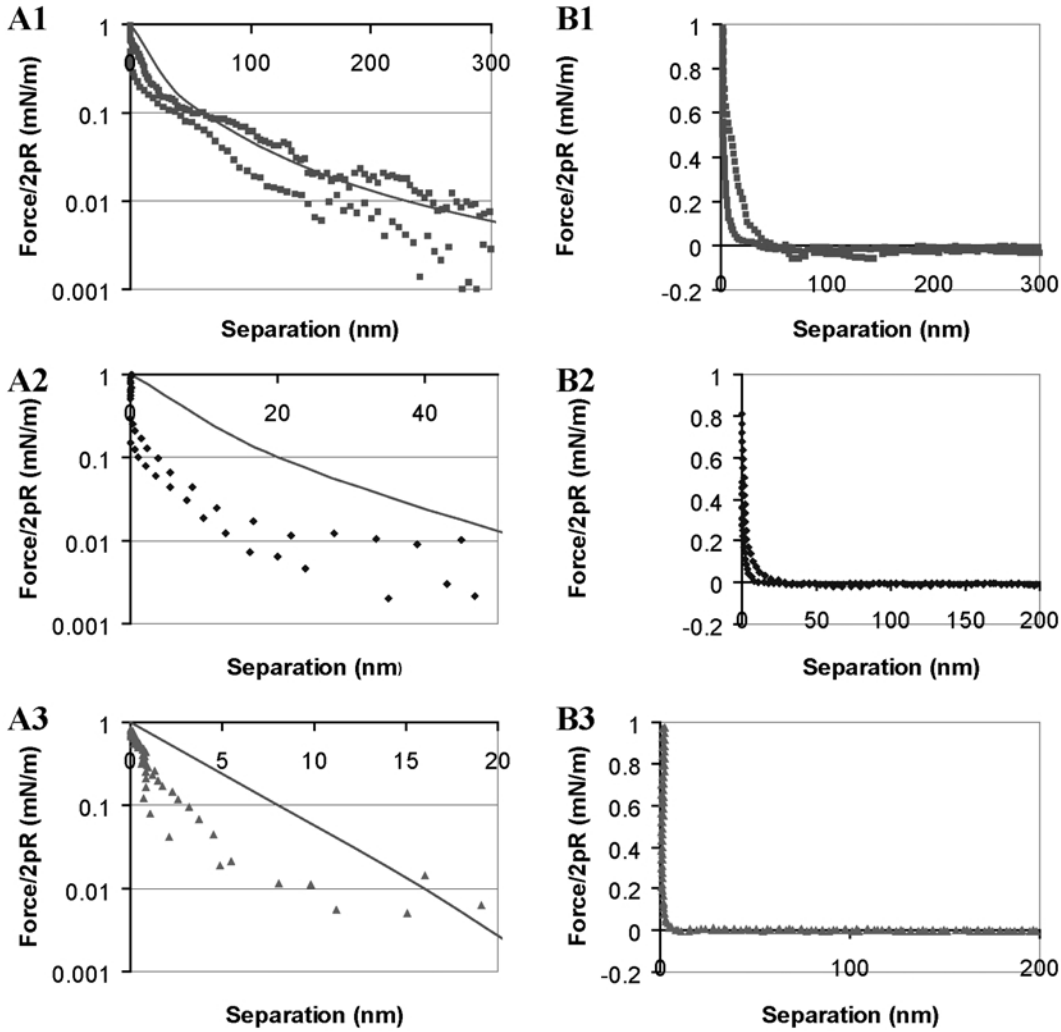

FIG. 4. Force–separation curves on approach (A series) and withdrawal (B series) for the interaction between platelets in the NP clay sample in water (A1, B1), in 0.01 M KCl (A2, B2) and in 0.1 M KCl (A3, B3). The solid lines in the force measurement on approach represent forces measured between the silica probe and the bare mica surface at the relevant KCl electrolyte concentration.

According to the Poisson and Boltzmann equations, one of the most characteristic parameters is the Debye length which represents the thickness of the double layer. At constant temperature and dielectric permittivity, the thickness of the diffuse double layer depends only on the ionic strength.

In the case of the NP clay sample deposited on a silicon wafer, the repulsion force in water at long range has been recorded when approached (Fig. 4, A1) from relatively large distance of separation ~150 nm. This may be due to the electrostatic interaction effect with the addition of a structural steric effect caused by the presence of smectite in this sample; this has recently been described by Żbik *et al*. (2008). Forces on the distance of separation of ~50 nm increases exponentially from 0.8 to 0.5 mN/m in water, which show a typical pattern of electrostatic repulsion. Measurement points in water closely follow mica electrostatic interactions, probably

arising from the large illite content in this sample. Electrolyte addition causes a significant reduction of force over similar distances of separation which is strong evidence of the electric double-layer interaction in this case. At electrolyte concentrations of 0.01 M KCl, repulsive forces were recorded from ~15 nm separation distance from the clay surface and increases exponentially to a value of 0.28 mN/m. Electric charge is here smaller than in mica interaction. At the greater electrolyte concentration 0.1 M KCl, the surfaces recorded repulsion from a distance of separation of ~4 nm and increased exponentially to a value of 0.8 mN/m. Also, the force measurement points are close to a solid line, representing electrostatic interaction with mica surfaces of the same electrolyte strength.

For the curves showing surface separation on withdrawal in the studied clay sample (Fig. 4, B series), only repulsion forces have been recorded and it was observed qualitatively that no adhesion had occurred, i.e. the clay platelets did not attach to each other in water and in electrolyte of 0.01 and 0.1 M salt concentration. However, over many of the curves studied, some show slight adhesion in 0.1 M electrolyte. On average, force curves on withdrawal are similar to these recorded when a colloidal probe approached the clay surface. This is typical of hydrophilic interaction, where electrostatic repulsion of an electric double layer prevails.

It is also possible that these long-distance forces observed in water, similar to electrostatic repulsion, have a steric origin and reflect the flexibility of smectite flakes detected in XRD patterns of a gel layer which may form as the outermost layer on top of a clay film on a substrate submerged in water. In effect, hindrance of other platelets against the interaction between the two platelets involved would be unavoidable.

In the case of the P clay sample deposited on silicon wafers, repulsion forces in water are also recorded as the approach occurs (Fig. 5) from relatively large distance of separation ~150 nm; this is similar to that recorded in the NP clay sample. However, the force increase is not exponential and the measurement points lay below the line which represents forces measured between silica probe and bare mica surface in water. Also, the force increases only to the limited value of 0.4 mN/m. This may suggest a lower electric charge in comparison with the NP clay sample. Electrolyte addition again causes a significant reduction of force over a distance of separation, which is further evidence of the electric double-layer interaction. In an electrolyte concentration 0.01 M KCl, attractive forces were recorded from distances of ~35 nm. These attractive forces brought the surfaces to a separation distance of ~8 nm. Then repulsive forces were recorded from 8 nm clay surface separation and forces increased to a value of 0.38 mN/m. Similar to the measurements made in water, possible hydrophobic interaction refining the force curves in comparison with similar curves were recorded for the NP clay sample. At greater electrolyte concentration, the 0.1 M KCl surfaces recorded attractive forces from distance of ~25 nm and repulsive forces from a distance of 5 nm. The repulsive force increased to lower value of 0.28 mN/m. Strong suppression of negative charge is easily observed when comparing this curve with that obtained from pure mica interaction as well as that from the NP clay sample. A distance of separation of ~5−8 nm is characteristic in this experiment to the hydrocarbon chains attached to clay particle surfaces.

The curves recorded on separation in the P clay sample (Fig. 5) show very strong adhesion which correlates poorly to the electrolyte strengths. It shows that adhesion increases with a decrease in the ionic strength of the electrolyte. This is a feature that has previously been observed between hydrophobic surfaces and attributed to the presence of tiny air micro-bubbles or hydrocarbon chains attached to the hydrophobic (and probably slightly rough) surfaces (Carambassis *et al.*, 1998; Considine *et al.*, 1999). This surface feature can be caused by the hydrophobic action of hydrocarbon blankets, but as soon as this blanket is contacted, a bridge forms between the surfaces and pulls the surfaces together rapidly. In the present system, it is not clear whether the surfaces are bridged by air, micro-bubbles, hydrocarbons, or by complex clay film, or mixtures of these. What is clear is that when they are brought to within a separation of a few nanometers, the clay-coated sphere becomes attached to the clay-coated substrate. The observed jump to a contact can be described as hydrophobic behaviour and it was also observed in electrolytes in the P clay sample when the colloidal probe approached the surface.

Strong adhesion between clay particles measured in the polluted soil sample P infers that micro-bubbles were only partly removed from the clay particle surfaces by ultrasonic action during sample redispersion in water. It is also possible that the

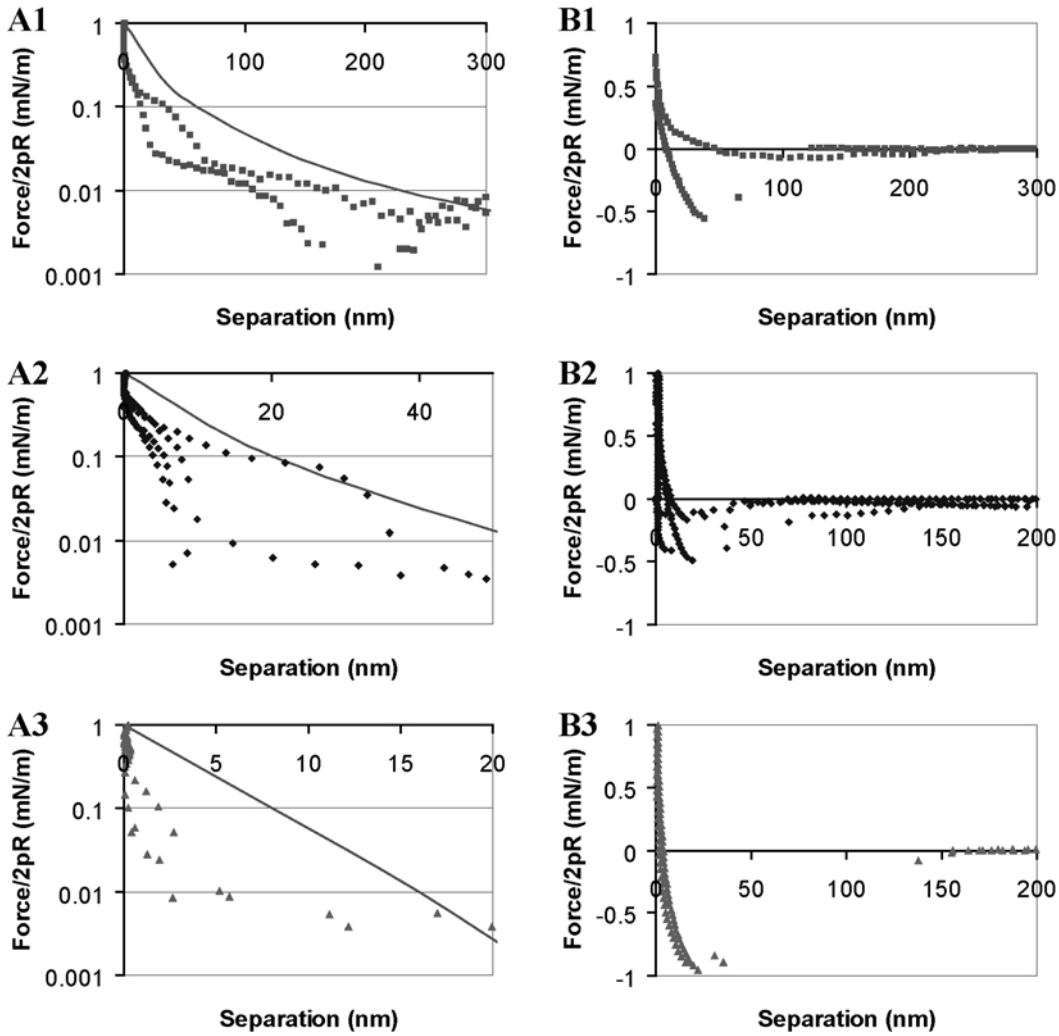

FIG. 5. Force–separation curves on approach (A series) and withdrawal (B series) for the interaction between platelets in the P clay sample in water (A1, B1), in 0.01 M KCl (A2, B2), and in 0.1 M KCl (A3, B3). The solid lines in the force measurement on approach represent forces measured between the silica probe and the bare mica surface at the relevant KCl electrolyte concentration.

observed adhesion may be the result of the presence of hydrocarbon chains on the clay surfaces and in solution, rather than by micro-bubble interactions. Force curves recorded on withdrawal (Fig. 5) in every case show adhesion on separation, i.e. the clay film forming the clay–hydrocarbon bridges must be ruptured by relatively strong forces of magnitude of 0.6–0.8 mN/m when the surfaces are close enough and before they can be violently separated and increased to rather large distances of ~100–200 nm separation.

Polluted clay due to diesel spillage shows lower repulsive forces on approach and strong adhesion on separation. This influences the processes of particle aggregation. Due to suppression of electrostatic repulsive forces and presence of strong adhesion between clay particles, they tend to flocculate, which was observed in sedimentation tests. When exposed to the pure diesel oil, clay particles formed larger aggregates which acted as silt/sand grains and settled out of the suspension rapidly. This aggregate building effect is reflected

in the polluted soil microstructure. In the polluted sample, particles are bonded to each other by cohesion into larger forms, loosely arranged through the sample, giving larger, inter-aggregate voids. On the contrary, in unpolluted samples the micro-structure shows strong particle interaction and smaller voids, where particles are bonded by strong electrostatic forces.

CONCLUSIONS

1. The particle size distribution of the soil in water and in diesel oil revealed strong flocculation of particles and rapid settlement of the silty aggregates formed in the diesel oil environment.

2. The unpolluted soil has a comparatively medium packed matrix type of microstructure dominated by FF, EE contacts and smaller, elongated intermicroaggregate/interparticle pores. By contrast, in the polluted soil, the clayey matrix is more loosely packed and disintegration/rearrangement of natural aggregates was observed. There were more EF contacts and larger and more isometric pores opened.

3. he quantitative analysis of micrographs showed substantial differences in the morphometric and geometrical parameters of the pore space between polluted and unpolluted soils. In polluted soil, the total pore number was lower, but the maximum and average values of pore area, perimeter and diameter increased, which is related to the increased number of mesopores. The polluted soil microstructure proved to be more isotropic and less oriented. A smaller number of fissure pores and a lower anisotropy index was observed in polluted soil.

4. The AFM force measurements have produced clear qualitative information about the interaction between the uncontaminated clay sample (NP) in water and KCl salt solutions of 0.01 M and 0.1 M ionic strength. Repulsive double-layer forces were measured between all the surfaces studied, which demonstrates that the uncontaminated clay sample NP is also negatively charged in water. The repulsive force is strong enough to prevent attachment of clays to each other at the electrolyte concentrations studied. The exponential nature of the force increases as a function of distance in the clay samples and shows a typical electrostatic repulsion of electric double layers on hydrophilic interfaces where the curves on approach are similar to these recorded during colloidal probe withdrawal.

5. The presence of strong adhesion on approach and withdrawal in hydrocarbon contaminated sample P suggests that micro-bubbles were probably removed from the clay particle interface by ultrasonic action during the sample dispersion in water. The observed hydrophobic adhesion may be the result of the presence of hydrocarbon chains on the clay surfaces and in the solution rather than micro-bubble interactions.

6. Electrostatic interaction forces in oil-polluted samples were much smaller than that measured in the case of clean samples with lower repulsive forces on approach and they generate strong adhesion on withdrawal in comparison with unpolluted samples. As a consequence, oil-polluted clays display more open porosity and larger void diameters than unpolluted samples which are characterized by the occurrence of the strong electrostatic interaction between particles.

7. Force action resulted micro-structures showing strong particle interaction and smaller voids when strong electrostatic forces bonding in unpolluted samples and larger voids in polluted samples where electrostatic interaction was suppressed by long-lasting hydrophobic blanketing.

ACKNOWLEDGMENTS

The Faculty of Geology, University of Warsaw, is thanked for financial support (project BW 1797/ 7). The authors are also grateful to Cecylia Szyszko and Leszek Kieszczyński for help in laboratory testing.

REFERENCES

ASTM (1990) *Annual Book of ASTM Standards.* American Society for Testing and Materials, Philadelphia, D422.

ASTM (2006) *Annual Book of ASTM Standards.* American Society for Testing and Materials, Philadelphia, D2487.

Berger W., Kalbe U. & Goebbels J. (2002) Fabric studies on contaminated mineral layers in composite liners. *Applied Clay Science*, **21**, 89–98.

Bowders J.J. & Daniel D.E. (1987) Hydraulic conductivity of compacted clay to dilute organic chemicals. *Journal of Geotechnical Engineering*, ASCE, **113**, 1432–1448.

BS (1990) *British Standards Institution*, London. 1377: Part 2: 9.5.

Carambassis A., Jonker L.C., Attard P. & Rutland M.W. (1998) Forces measured between hydrophobic surfaces due to a submicroscopic bridging bubble. *Physical Review Letters*, **80**, 5357–5360.

Considine R.F., Hayes R.A. & Horn, R.G. (1999) Forces measured between latex spheres in aqueous electrolyte: non-DLVO behavior and sensitivity to dissolved gas. *Langmuir*, **15**, 1657–1659.

Ducker W.A., Senden T.J. & Pashley R.M. (1991) Direct measurement of colloidal forces using an atomic force microscope. *Nature*, **353**, 239–241.

Fang H.Y. (1997) *Introduction to Environmental Geotechnology.* CRC Press, Boca Raton, Florida, USA.

Fernandez F. & Quigley R.M. (1985) Hydraulic conductivity of natural clays permeated with simple liquid hydrocarbons. *Canadian Geotechnical Journal*, **22**, 205–214.

Fernandez F. & Quigley R.M. (1988) Viscosity and dielectric constant controls on the hydraulic conductivity of clayey soils permeated with water-soluble organics. *Canadian Geotechnical Journal*, **25**, 582–589.

Gillott J.E. (1987) *Clay in Engineering Geology.* Developments in Geotechnical Engineering, **41**, Elsevier, Amsterdam – Oxford – New York – Tokyo.

Grabowska-Olszewska B., Osipov V.I. & Sokolov V.N. (1984) *Atlas of Microstructure of Clay Soils*. Państwowe Wydawnictwo Naukowe, Warszawa, Poland.

Izdebska-Mucha D. (2005) Influence of oil pollution on geological-engineering properties of clay soils. *Przegląd Geologiczny*, **53**, 766–769 (in Polish with English abstract).

Izdebska-Mucha D. & Trzciński J. (2008) Effects of petroleum pollution on clay soil microstructure. *Geologija*, **50**, 68–74.

Kaya A. & Fang H.Y. (2000) The effects of organic fluids on physicochemical parameters of fine-grained soils. *Canadian Geotechnical Journal*, **37**, 943–950.

Kaya A. & Fang H.Y. (2005) Experimental evidence of reduction in attractive and repulsive forces between clay particles permeated with organic liquids. *Canadian Geotechnical Journal*, **42**, 632–640.

Khamehchiyan M., Charkhabi A.H. & Tajik M. (2007) Effects of crude oil contamination on geotechnical properties of clayey and sandy soils. *Engineering Geology*, **89**, 220–229.

Korzeniowska-Rejmer E. & Izdebska-Mucha D. (2006) Evaluation of the influence of oil pollution on particle size distribution and plasticity of clay soils. *Inżynieria i Ochrona Środowiska*, **9**, 89–103 (in Polish with English abstract).

Mitchell J.K. (1976) *Fundamentals of Soil Behaviour.* John Wiley and Sons, New York.

Moavenian M.H. & Yasrobi S.S. (2008) Volume change behavior of compacted clay due to organic liquids as permeant. *Applied Clay Science*, **39**, 60–71.

Riser-Roberts E. (1998) *Remediation of Petroleum Contaminated Soils.* Lewis Publishers, London.

Sergeyev Y.M., Grabowska-Olszewska B., Osipov V.I., and Sokolov V.N. (1978) Types of the microstructures of clayey soils. *Proceedings of the III International Congress I.A.E.G.*, **1**, 319–327.

Sergeyev Y.M., Grabowska-Olszewska B., Osipov V.I., Sokolov V.N. & Kolomenski Y.N. (1980) The classification of microstructure of clay soil. *Journal of Microscopy*, **120**, 237–260.

Sergeyev Y.M., Spivak G.V., Sasov A.Y., Osipov V.I., Sokolov V.N. & Rau E.I. (1983) Quantitative morphological analysis in a SEM microcomputer system II. Morphological analysis of complex SEM images. *Journal of Microscopy*, **135**, 13–24.

Singh S.K., Srivastava R.K. & John S. (2009) Studies on soil contamination due to used motor oil and its remediation. *Canadian Geotechnical Journal*, **46**, 1077–1083.

Smart P. & Tovey N.K. (1982) *Electron Microscopy of Soils and Sediments: Techniques.* Clarendon Press, Oxford.

Sokolov V.N., Yurkovets D.I. & Razgulina O.V. (2002) *Stiman (Structural Image Analysis): a Software for Quantitative Morphological Analysis of Structures by their Images* (User's Manual, Version 2.0). Laboratory of Electron Microscopy, Moscow State University Press, Moscow, Russia.

Surygała J.& Śliwka E. (1999) Wycieki ropy naftowej. *Przemysł Chemiczny*, **78**, 323–325.

Tovey N.K. & Wong K.Y. (1973) The preparation of soils and other geological materials for the S.E.M. Pp. 59–67 in: *Proceedings of the International Symposium on Soil Structures*. Swedish Geotechnical Society, Stockholm.

Trzciński J. (2004) Combined SEM and computerized image analysis of clay soils microstructure: technique & application. Pp. 654–666 in: *Advances in Geotechnical Engineering: the Skempton Conference* (R.J. Jardine, D.M. Potts & K.G. Higgins, editors) **1**, Thomas Telford, London.

Trzciński J. (2008) Microstructure and physico-mechanical properties of tills in Poland. *Geologija*, **50**, 26–39.

Uppot J.O. & Stephenson R.W. (1989) Permeability of clays under organic permeants. *Journal of Geotechnical Engineering*, ASCE, **115**, 115–131.

Żbik M.S. & Frost R.L. (2010) Influence of smectite suspension structure on sheet orientation in dry sediments: XRD and AFM applications. *Journal of Colloid and Interface Science*, **346**, 311–316.

Żbik M.S., Martens W., Frost R.L., Song Y.F., Chen Y.M. & Chen J.H. **(**2008) Transmission X-ray microscopy (TXM) reveals the nanostructure of a smectite gel. *Langmuir*, **24**, 8954–8958.